Int. J. Adv. Appl. Math. and Mech. 8(3) (2021) 48 – 61 (ISSN: 2347-2529)

Journal homepage: www.ijaamm.com

IJAAMM

International Journal of Advances in Applied Mathematics and Mechanics

# A Spectral-based Numerical Study on Time-dependent Fluid Flow and Energy Distribution through a Rotating Coiled Rectangular Duct with the Effects of Coriolis Force

**Research Article**

**Ratan Kumar Chanda[a], Md. Kutub Uddin[b], Rabindra Nath Mondal[a,] ***

[a] *Department of Mathematics, Jagannath University, Dhaka-1100, Bangladesh*

[b] *Department of Mathematics, University of Dhaka, Dhaka-1000, Bangladesh*

**Received 30 November 2020; accepted (in revised version) 05 February 2021**

**Abstract:** The present paper deals with a spectral-based numerical study on unsteady flow characteristics and temperature distribution through a tightly coiled rectangular duct of curvature ratio 0.5 with the effects of Coriolis force. The outer wall of the duct is heated while the inner wall in room temperature. A rotation of the duct about the vertical axis is imposed in the negative direction for the Taylor number $-1000 \leq Tr < 0$ applying a constant pressure gradient force, the Dean number (Dn), along the axial direction. In order to study the unsteady behavior of the flow, time-history analysis is performed and flow transition is precisely determined by obtaining phase space of the time-evolution results. It is found that the unsteady flow undergoes in the state 'chaotic multi→ periodic → periodic → steady-state', if Tr is increased in the negative direction. Streamlines of secondary flow and isotherms of temperature distributions are obtained at several values of Tr, and it is found that the unsteady flow consists of asymmetric 2- to 6-vortex solutions. The present study shows that convective heat transfer (HT) is significantly enhanced by the secondary flow; and the chaotic flow, which occurs relatively at small Tr but at large Dn, enhances heat transfer more effectively than the steady-state or periodic solutions. Finally, our numerical results have been validated with experimental outcomes and it is found that there is a good agreement between the numerical and experimental investigations.

**MSC:** 76D05 • 76U05

**Keywords:** Rotating curved duct • Taylor number • Secondary flow • Periodic solution • Isotherm



## 1. Introduction

The study of rotating fluids flow characteristics through a RCD is highly important because of its occurrence in various natural phenomena and technological situations such including chemical reactors, rocket engines, aircraft engines, gas turbines, air-conditioning, refrigeration, turbo-machinery but also used in biological problems such as in human Lung, blood circulation in vein and arteries. It is recognized that there is a basic difference between straight channel flow and curved duct flow in terms of creating forces. CD generates two types of forces; one is the centrifugal force causing duct curvature and the other is Coriolis force due to rotation. The work of centrifugal body force is mainly on the outer concave wall of the duct because of the pressure gradient of the flow. Consequently, the generation of two-vortex secondary flow is transferred into four-vortex under a critical flow condition. These types of vortices were first noticed by Dean [1] which is called Dean vortices after his name and the flow instability is known

* Corresponding author.
*E-mail address(es):* rnmondal71@yahoo.com (Rabindra Nath Mondal)

**Nomenclature**

| | |
|---|---|
| $Dn$ | Dean number |
| $g$ | Gravitational Acceleration |
| $Gr$ | Grashof number |
| $G$ | Mean pressure gradient |
| $Tr$ | Taylor number |
| $Pr$ | Prandtl number |
| $L$ | Radius of the curvature |
| $T$ | Temperature |
| $t$ | Time |
| $Ar$ | Aspect ratio |
| $h$ | Half-height of the cross section |
| $d$ | Half-width of the cross section |
| $u, v, w$ | Velocity components in the x, y, z direction respectively |
| $x, y$ | Rectangular coordinate axes |
| $z$ | Axis in the working fluid flow direction |

*Greek symbols*

| | |
|---|---|
| $\delta$ | Curvature of the duct |
| $\lambda$ | Resistance coefficient |
| $\kappa$ | Thermal diffusivity |
| $\psi$ | Sectional stream function |
| $\rho$ | Density |
| $\mu$ | Viscosity |
| $\nu$ | Kinematic viscosity |

*Abbreviations*

| | |
|---|---|
| CD | Curved duct |
| RCD | Rotating curved duct |
| SD | Straight duct |
| HT | Heat transfer |
| CHD | Convective Heat transfer |

as hydrodynamic instability. The fluid flow problems in rotating medium have drawn attention of many researchers who investigated hydrodynamic flow of a viscous and incompressible fluid in rotating medium considering different aspects of the problem. The emergence and accessibility of increasingly inexpensive computing power have dramatically advanced the research on numerical treatment of the flow through the duct in the last few decades, a series of landmark reviews on curved duct flows, use various configurations, are given by Humphery et al. [2] for square and rectangular cross-sections, Ghia and Sokhey [3] for rectangular cross-section, Yanase et al. [4] for rectangular duct, Chandratilleke et al. [5] for rectangular and elliptical curved ducts.

Flow structure characteristics through a CD are widely used in metallic and petroleum engineering. Both two- and three-dimensional studies on the fluid flow through the square duct have been examined by Yanase et al. [6]. Yamamoto et al. [7] represented the secondary flow profiles for a wide range of Dean and Taylor numbers. A comprehensive study of spiraling fluid flow properties and HT in the flow through a CRD from experimental and numerical points of view was presented by Chandratilleke and Nursubyakto [8] for small Dn and compared the numerical results with their experimental data. Mondal et al. [9] have compared their numerical results with the experimental data that obtained by Chandratilleke et al. [10] and visualized the stream functions and the isotherms for different Dean and Grahof numbers. The buoyancy forces in the curved duct are converted into the driving force for the secondary flow, which has been obtained by Wang et al. [11]. Recently, flow characteristics, heat transfer and entropy generation has been performed by Razavi et al. [12]. Heat transfer in both steady and unsteady solutions with temperature gradients in the RCD has been calculated by Hasan et al. [13]. Rivas et al. [14] have explained the turbulent forced convection coupled to heat conduction in a cross-section of square duct. Norouzi et al. [15] have elaborated first and second normal stresses with enumerating the Nusselt number and the influence on secondary flow intensity in the elastic property. Mondal et al. [16] inspected a spectral-based numerical study for two-dimensional viscous incompressible fluid flow through a curved rectangular duct in a rotating system and showed that unsteady flow becomes chaotic if the aspect ratio is increased no matter what the rotational speed is. They obtained four- to twelve-vortex solutions and revealed that the axial flow shifts near the outer wall if the rotational speed is increased in the positive direction.

To solve the Navier-Stokes equations numerically, various parameters are considered to reveal the transient behaviors of the unsteady flow. In 1988, Yanase and Nishiyama [17] first analyzed the transient behavior of curved channel flow for rectangular cross section. From that time, several researchers have studied the flow behaviors using numer-

ical and experimental techniques. Very recently, time-dependent behavior with respect to the Drag Coefficient with their power spectrum and the vorticity contours has been visualized by Nazeer et al. [18]. For solving the unsteady flow through a curved tube with strong curvature, recently Krishna et al. [19] performed flow visualization and computational fluid dynamics. Mondal et al. [20, 21] performed numerical prediction of isothermal flow with unsteady solutions through a stationary curved square duct. The main finding of their study was that periodic solutions transform into chaotic via multi-periodic solution for increasing Dean number and independent of the curvature. In a separate study, Mondal et al. [22] reported profound effect of Dean number and the Grashof number on the flow transition using numerical method. Islam et al. [23] showed transitional behavior of the flow in a rotating curved duct for various Dean numbers over a wide range of Taylor number. Iva et al. [24] applied explicit finite difference method to investigate unsteady free convection heat and mass transfer flow past a semi-infinite vertical porous plate in a rotating system. They showed that the solution is dependent on several governing parameters including the magnetic parameter, heat source parameter, Grashof number, modified Grashof number, hall parameter, Prandtl number, Schmidt number, wall temperature and concentration exponent. Understanding the transition phenomenon may help in more efficient designs for mixing and heat transfer applications. There are also many situations where the flow is required to remain in a laminar state to reduce the skin friction drag. For all these applications, it is necessary to have a better understanding of the transition process. But still, transition is one of the least understood areas of fluid mechanics due to the complex spatiotemporal nature of the flow during transition. The present study focuses on the transition for the flow through a rotating curved rectangular duct with strong Coriolis force.

To progress the understanding of thermo-fluid behavior and heat transfer in a curved channel, Chandratilleke and Nursubyakto [8] presented a numerical study in externally heated curved rectangular ducts with $1 \leq Ar \leq 8$. It was shown that the number of Dean vortices formed is strongly influenced by aspect ratio and convective heat transfer is significantly enhanced by the secondary flow. More recently, Chandratilleke et al. [25] proposed an improved model based on 3-dimensional (3D) vortex structures to capture the onset of hydrodynamic instability and resulting Dean vortices in a curved rectangular duct with various aspect ratios and curvatures. The results showed that aspect ratio strongly influences the number of Dean vortices formed, based on assigned helicity threshold and adverse pressure gradient at outer duct wall to identify Dean vortex generation. The effect of secondary motion on the heat and mass transfer has been investigated in numerical simulations of turbulent duct flows with mixed convection by Niemann et al. [26] and Sekimoto et al. [27]. Recently, Hasan et al, [28, 29] conducted numerical prediction of fluid flow and heat transfer through a rotating and non-rotating (separate study) curved square channel for various curvatures. The main findings of the both studies were that time-dependent flow undergoes through various flow instabilities for increasing Tr; the role of secondary vortices on convective heat transfer which was significantly enhanced by the secondary flow and the chaotic flow enhances heat transfer more efficiently than the steady-state or periodic solutions. Very recently, Roy et al. [30] investigated hydrodynamic instability and convective heat transfer through a CRD of moderate curvature for rotating system. They identified that chaotic flow turns into steady-state through periodic flow for increasing positive rotation. However, the complete work with the effects of secondary flow on unsteady behavior and convective heat transfer in a curved rectangular channel for negative rotation existing strong centrifugal as well as Coriolis instability has not yet been investigated, which is an important objective of the present study.

## 2. Flow Model and Governing Equations

### 2.1. Physical Model

A schematic drawing of the 2D physical model considered in the present study is shown in Fig. 1. The system consists of a CRD with vertical and horizontal sides of length 2h and 2d respectively. The fluid is assumed to be incompressible 2D flow. In this study, the CRD is immersed in a hydro-dynamically and thermally (outer wall heated and inner wall cooled, the top and bottom walls being adiabatic) fully developed flows with constant angular velocity (CAV) $\Omega_T$ around the vertical axis. We also consider that the flow passes through uniformly in the z-axis direction as presented in Fig. 1.

### 2.2. Governing equations

The dimensional variables are made non-dimensional by using the characteristic length d and velocity scale $U_0$, defined by $U_0 = \frac{\upsilon}{d}$, where $\upsilon$ is the kinematic viscosity of the fluid. The stream functions for cross-sectional velocities have the following form

$$\left.\begin{aligned} u &= \frac{1}{r}\frac{\partial \psi}{\partial y} = \frac{1}{1+\delta x}\frac{\partial \psi}{\partial y} \\ v &= \frac{1}{r}\frac{\partial \psi}{\partial x} = -\frac{1}{1+\delta x}\frac{\partial \psi}{\partial x} \end{aligned}\right\} \tag{1}$$

Then, basic equations for $w, \psi$, and $T$ are derived from the Navier–Stokes equations and energy equation as follows

$$(1+\delta x)\frac{\partial w}{\partial t} = Dn - \frac{1}{2}\frac{\partial(w,\psi)}{\partial(x,y)} - \frac{\delta^2 w}{1+\delta x} + (1+\delta x)\Delta_2 w - \frac{1}{2}\frac{\delta}{(1+\delta x)}\frac{\partial \psi}{\partial y}w + \delta\frac{\partial w}{\partial x} - \delta Tr\frac{\partial \psi}{\partial y} \tag{2}$$

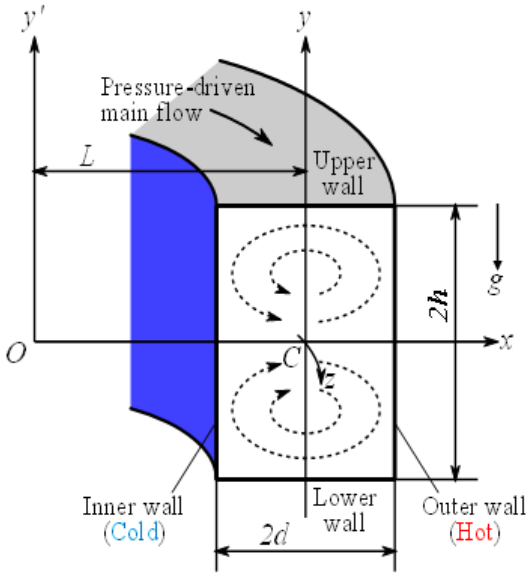


**Fig. 1.** Schematic representation of Computational domain

$$\left(\Delta_2-\frac{\delta}{1+\delta x}\frac{\partial}{\partial x}\right)\frac{\partial\psi}{\partial t}=-\frac{1}{2}\frac{1}{(1+\delta x)}\frac{\partial(\Delta_2\psi,\psi)}{\partial(x,y)}+\frac{1}{2}\frac{\delta}{(1+\delta x)^2}\times\left[\frac{\partial\psi}{\partial y}\left(2\Delta_2\psi-\frac{3\delta}{1+\delta x}\frac{\partial\psi}{\partial x}+\frac{\partial^2\psi}{\partial x^2}\right)-\frac{\partial\psi}{\partial x}\frac{\partial^2\psi}{\partial x\partial y}\right]+\frac{\delta}{(1+\delta x)^2}\times\left[3\delta\frac{\delta^2\psi}{\partial x^2}-\frac{3\delta^2}{1+\delta x}\frac{\partial\psi}{\partial x}\right]-\frac{2\delta}{1+\delta x}\frac{\partial}{\partial x}\Delta_2\psi+\Delta_2^2\psi+\frac{1}{2}w\frac{\partial w}{\partial y}-Gr(1+\delta x)\frac{\partial T}{\partial x}-\frac{1}{2}Tr\frac{\partial\psi}{\partial y},\tag{3}$$

$$\frac{\partial T}{\partial t}=\frac{1}{\mathrm{Pr}}\left(\Delta_2 T+\frac{\delta}{1+\delta x}\frac{\partial T}{\partial x}\right)-\frac{1}{(1+\delta x)}\frac{\partial(T,\psi)}{\partial(x,y)}\tag{4}$$

where

$$\Delta_2\equiv\frac{\partial^2}{\partial x^2}+\frac{1}{4}\frac{\partial^2}{\partial y^2},\quad\frac{\partial(f,g)}{\partial(x,y)}\equiv\frac{\partial f}{\partial x}\frac{\partial g}{\partial y}-\frac{\partial f}{\partial y}\frac{\partial g}{\partial x}.\tag{5}$$

The system is therefore governed by the following four non-dimensional parameters which are included in equations (2) - (4) defined as

$$Dn=\frac{Gd^3}{\mu\upsilon}\sqrt{\frac{2d}{L}},\quad Tr=\frac{2\sqrt{2\delta}\Omega_T d^3}{\upsilon\delta},\quad Gr=\frac{\beta g\Delta T\,d^3}{\upsilon^2},\quad \mathrm{Pr}=\frac{\upsilon}{\kappa}\tag{6}$$

The non-dimensional boundary conditions for fluid axial velocity and secondary flow are:

$$w(\pm1,y)=w(x,\pm1)=\psi(\pm1,y)=\psi(x,\pm1)=\frac{\partial\psi}{\partial x}(\pm1,y)=\frac{\partial\psi}{\partial y}(x,\pm1)=0\tag{7}$$

and the temperature $T$ is assumed to be constant on the walls as

$$T(1,y)=1,\quad T(-1,y)=-1,\quad T(x,\pm1)=x\tag{8}$$

In the present study, water is the working fluid ($Pr=7.0$) and $Tr$ varies in the negative direction, while $Dn, Gr$ and $\delta$ are fixed as $Dn=1500, Gr=100, \delta=0.5$

## 3. Numerical analysis

### 3.1. Numerical procedure

In order to find the numerical solution of equations (2) - (4), spectral method is used which is the best numerical scheme for solving the Navier-Stokes as well as energy equations (Gottlieb and Orszag [31]). By this method the variables are expanded in a series of functions consisting of the Chebyshev polynomials. That is, the expansion functions $\varphi_n(x)$ and $\psi_n(x)$ are stated as

$$\left.\begin{aligned}\varphi_n(x)&=(1-x^2)\,C_n(x),\\ \psi_n(x)&=(1-x^2)^2C_n(x)\end{aligned}\right\}\tag{9}$$

where $C_n(x) = \cos(n\cos^{-1}(x))$ is the $n^{th}$ order Chebyshev polynomial. $w(x,y,t)$, $\psi(x,y,t)$ and $T(x,y,t)$ are stated $\varphi_n(x)$ and $\psi_n(x)$ as:

$$\left.\begin{aligned} w(x,y,t) &= \sum_{m=0}^{M}\sum_{n=0}^{N} w_{mn}(t)\,\phi_m(x)\,\phi_n(y) \\ \psi(x,y,t) &= \sum_{m=0}^{M}\sum_{n=0}^{N} \psi_{mn}(t)\,\psi_m(x)\,\psi_n(y). \\ T(x,,y,t) &= \sum_{m=0}^{M}\sum_{n=0}^{N} T_{mn}\,\phi_m(x)\,\phi_n(y) + x \end{aligned}\right\} \tag{10}$$

where $M$ and $N$ represent the truncation numbers in the $x$ - and $y-$directions respectively, and $w_{mn}$, $\psi_{mn}$ and $T_{mn}$ are the coefficients of expansion. The collocation points $(x_i, y_j)$ are taken to be

$$x_i = \cos\left[\pi\left(1-\frac{i}{M+2}\right)\right], \quad y_j = \cos\left[\pi\left(1-\frac{j}{N+2}\right)\right] \tag{11}$$

where $i = 1,\ldots, M+1$ and $j = 1,\ldots, N+1$. In order to calculate the unsteady solutions, the Crank-Nicolson and Adams-Bashforth methods together with the function expansion (10) and the collocation methods are applied to Eqs. (2) to (4). Details of the method are available in Mondal [21].

### 3.2. Resistance Coefficient

The resistance coefficient $\lambda$, another name *hydraulic resistance coefficient* and denoting the quantity of the flow state, generally used in fluids engineering, defined as

$$\frac{{P_1}^* - {P_2}^*}{\Delta z^*} = \frac{\lambda}{{d_h}^*}\frac{1}{2}\rho\langle w^*\rangle^2 \tag{12}$$

In this relation, $^*$ in header of each parameter mentions to a dimensional parameter, $\langle\rangle$ position for the mean over the cross section of the duct and ${d_h}^*$ is the *hydraulic diameter*. The mean axial velocity $\langle w^*\rangle$ is deliberated by

$$\langle w^*\rangle = \frac{\nu}{4\sqrt{2\delta}\,d}\int_{-1}^{1} dx \int_{-1}^{1} w(x,y,t)\,dy. \tag{13}$$

Since $({P_1}^* - {P_2}^*)/\Delta z^* = G$, $\lambda$ is linked to the mean non-dimensional axial velocity $\langle w\rangle$ as

$$\lambda = \frac{16\sqrt{2\delta}\,Dn}{3\langle w\rangle^2}, \tag{14}$$

where $\langle w\rangle = \sqrt{2\delta}\,d\langle w^*\rangle/\nu$.

## 4. Results and discussion

Numerical simulations of non-linear behavior of the transient solutions in a CRD are performed to study the effects of the Taylor number (Tr), the Dean number (Dn), the Grashof number (Gr) and curvature ($\delta$) on the flow features. The simulations are performed in the following range of governing parameters as shown in Table 1. A detailed discussion on the initiation, development and transition of the flow characteristics with temperature distribution induced by the Taylor number is presented in the upcoming sections. We specify different regimes of Tr where the unsteady flow is steady-state, periodic, multi-periodic or chaotic as discussed below.

**Table 1.** Range of the governing parameters considered in the simulations.

| | |
|---|---|
| Grashof number ($Gr$) | 100 |
| Dean number ($Dn$) | 1500 |
| Curvature ($\delta$) | 0.5 |
| Tylor number ($Tr$) | $-1000 \le Tr < 0$ |
| Prandtl number ($Pr$) | 7.0 (water) |

### 4.1. Transient solution for $-600 \leq Tr < 0$

In this sub-section, a detailed examination of flow transient behavior for is presented. First, we investigate the oscillating behavior of $\lambda$ for Tr=-50, Tr=-100, Tr=-500 and Tr=-600 as depicted in Figs. 2(a), 3(a), 4(a) and 5(a) respectively, and it is found that the flow oscillates in the irregular pattern for the above mentioned values of Tr. To be confirm whether the flow is chaotic or not, we sketched the phase space (PS), and it is found that the chaotic orbits are crossed over the whole plane in a non-linear manner as shown in Figs. 2(b), 3(b), 4(b) and 5(b) for Tr=-50, -100,-500 and -600 respectively in the $\lambda - \gamma$ plane, where $\gamma = \int\int \psi dxdy$ that is the chaotic regime is obtained for $Tr \leq -600$. To monitor vortex-structure and isotherm, we attain velocity contours and isotherms as revealed in Figs. 2(c), 3(c), 4(c) and 5(c) for Tr=-50,-100,-500 and -600 respectively, where we see that the chaotic flow oscillates haphazardly in the asymmetric 1- to 6-vortex solution and mostly axial velocity is gathered near the outer bend of the duct. It is seen that increasing the number of secondary vortices the flow intensifies which causes the combined action of the strong centrifugal and Coriolis force as the rotational speed (Tr) is increased in the negative direction. In this study, temperature dis-

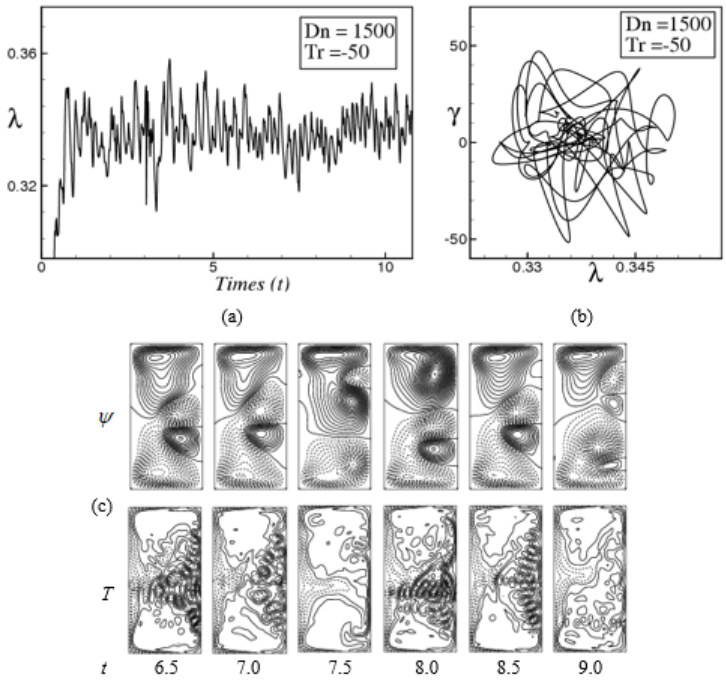


**Fig. 2.** Time-progress, phase-space and streamlines for Tr = -50 and $\delta = 0.5$. (a) Time advancement of $\lambda$, (b) Phase-portrait, (c) Contour plots of secondary flow (top), energy distribution (bottom) for $6.5 \leq t \leq 9.0$

tributions show that the streamlines of the heat flow is uniformly distributed to all parts of the contour transferring heat from outer wall to the fluid, and the contribution of the rotation and pressure on secondary flows significantly change and increase the number of secondary vortices. It is clearly evident that heating the outer wall causes the temperature contours to become asymmetrical in comparison to isothermal cases. This essentially arises from the interaction between the heating-induced buoyancy force and the centrifugal-Coriolis force that drives secondary vortices. In this regard, it should be noted that the centrifugal force due to the channel curvature creates two effects; it generates a positive radial fluid pressure field in the duct cross section and induces a lateral fluid motion driven from inner wall towards the outer wall. This lateral fluid motion occurs against the radial pressure field generated by the centrifugal effect and is superimposed on the axial flow to create the secondary vortex flow structure. As the flow through the curved duct is increased (larger Dn), the lateral fluid motion becomes stronger and the radial pressure field is intensified. In the vicinity of the outer wall, the combined action of adverse radial pressure field and viscous effects slows down the lateral fluid motion and forms a stagnant flow region. Beyond a certain critical value of Dn, the radial pressure gradient becomes sufficiently strong to reverse the flow direction of the lateral fluid flow. A weak local flow re-circulation is then established creating an additional pair of vortices in the stagnant region near the outer wall. This flow situation is known as Dean's hydrodynamic instability while the vortices are termed as Dean vortices. In this regard, it should be noted that, the occurrence of the chaotic state, as presented in the present study, is related with destabilization of the periodic or quasi-periodic solutions which reminds us the case of Lorenz attractor [32]. It may be possible that the transition in the present study is caused by a similar mechanism as that of Ruelle-Takens scenario [33] in the laminar flow. When the value of Tr is gradually increased in the negative direction at Tr = 620, the chaotic flow transforms into a multi-periodic flow. It is necessary to note that, transition from chaotic-state to multi-periodic

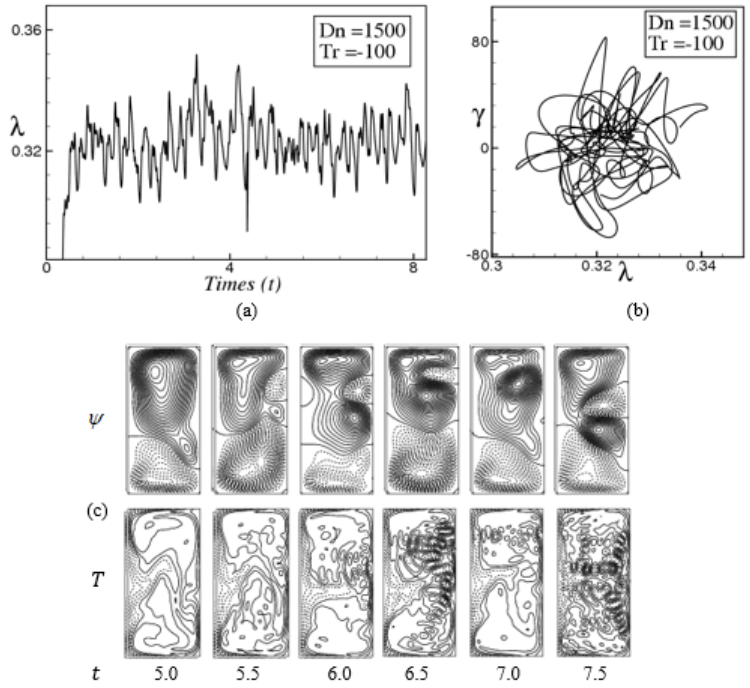


**Fig. 3.** Time-progress, phase-space and streamlines for Tr = -100 and $\delta = 0.5$. (a) Time advancement of $\lambda$, (b) Phase-portrait, (c) Contour plots of secondary flow (top), energy distribution (bottom) for $5.0 \leq t \leq 7.5$.

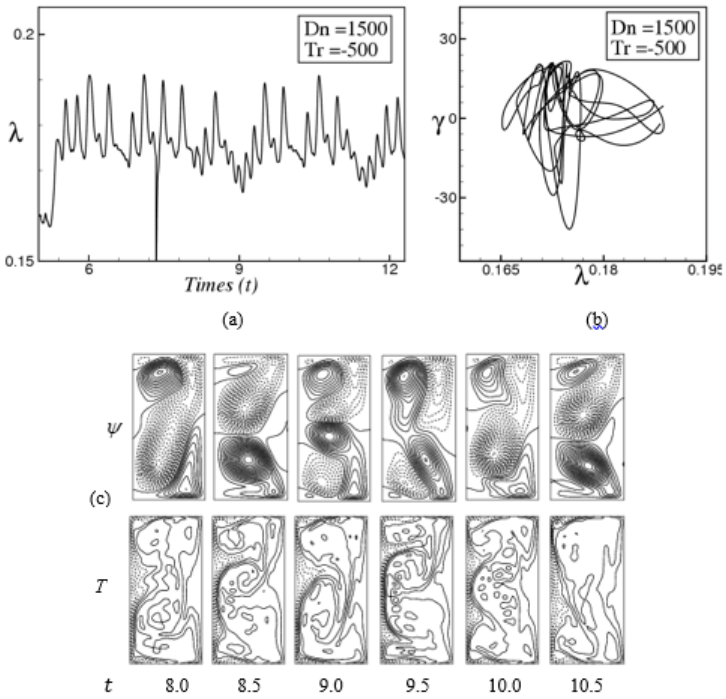


**Fig. 4.** Time-progress, phase-space and streamlines for Tr = -500 and $\delta = 0.5$. (a) Time advancement of $\lambda$ (b) Phase-portrait, (c) Contour plots of secondary flow (top), energy distribution (bottom) for $8.0 \leq t \leq 10.5$.

oscillation takes place between Tr = -600 and Tr = -620.

### 4.2. Transient solution for $-670 \leq Tr \leq -620$

We then searched for multi-periodic solution and we noticed that the unsteady flow is multi-period for $-670 \leq Tr \leq -620$. We calculate the time-evolution for the Taylor numbers from Tr = -670 to Tr = -620 as shown in Fig. 6(a) and

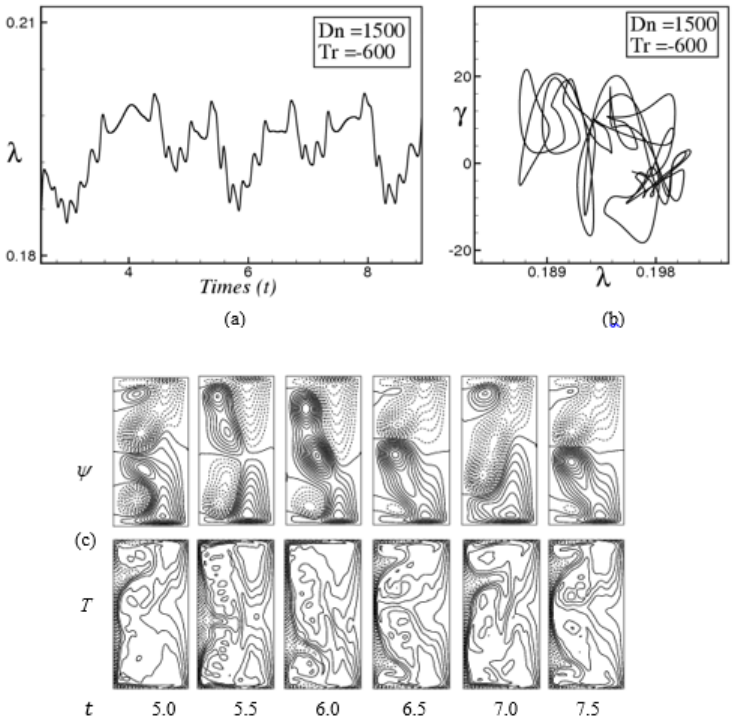


**Fig. 5.** Time-progress, phase-space and streamlines for Tr = -600 and $\delta = 0.5$. (a) Time advancement of $\lambda$, (b) Phase-portrait, (c) Contour plots of secondary flow (top), energy distribution (bottom) for $5.0 \leq t \leq 7.5$.

Fig. 7(a) respectively and multi-periodic oscillations are observed for all values from Tr = -620 to Tr = -670 justifing by depicting the PS ( refer to Fig. 6(b) and Fig. 7(b)) with axisymmetric two- to five- vortex solution for Tr = -620 and axisymmetric two- to four-vortex solution as shown in Figs. 6(c) and 7(c) respectively. The present study shows as Tr is increased gradually in the negative direction at Tr = -680, it is found that the multi-periodic flow turns into periodic flow as shown in Figure 8.

### 4.3. Transient solution for $Tr = -680$

With further increase of Tr in the negative direction, another flow transformation occurs at Tr = -680 where the multi-periodic flow transformed into a periodic flow as seen in Fig. 8(a) which is well justified by plotting the orbits of the solution in the PS as seen in Fig. 8(b), where we see that periodic orbits overlap each other creating a single cycle, which confirms that the flow at Tr = -680 is periodic. In this study we obtained no specefic region for periodic solution but at Tr = -680 only. In fact, the periodic oscillation, which is observed in the present study, is a traveling wave solution advancing in the downstream direction which is well-justified in the paper by Wang and Yang [18] and Yanase et al. [6] for three-dimensional travelling wave solutions as an appearance of 2D periodic oscillation. Therefore, it is suggested that 2D calculations can accurately predict the existence of 3D traveling wave solutions by showing an appearance of 2D periodic oscillation. The periodic oscillation at Tr = -680 consist of asymmetric two- and three-vortex solution. It is necessary to note that, transition from a multi-periodic flow to a steady-state takes place between Tr = -670 and Tr = -680. If Tr is increased in the negative direction further, for example Tr = -700, it is observed that the flow characteristics are suddenly changed, and the periodic solution turns into steady-state solution [see Fig. 9]

### 4.4. Transient solution for $-1000 \leq Tr \leq -700$

In order to search the region of steady-state solution, we deliberated transient solution for $-1000 \leq Tr \leq -700$. On further increasing the value of Tr another steady-state flow pattern with axisymmetric 2-vortex solution is observed at Tr = -700 (see Fig. 9). The same type of steady-state flow pattern is observed for $-1000 \leq Tr \leq -700$. It is perceived that the transition from periodic wavering to steady-state occurs between Tr = -680 and Tr = -700. It is also found that temperature distribution is consistent with secondary vortices, and secondary flow enhances heat transfer in the flow through vortex generation.

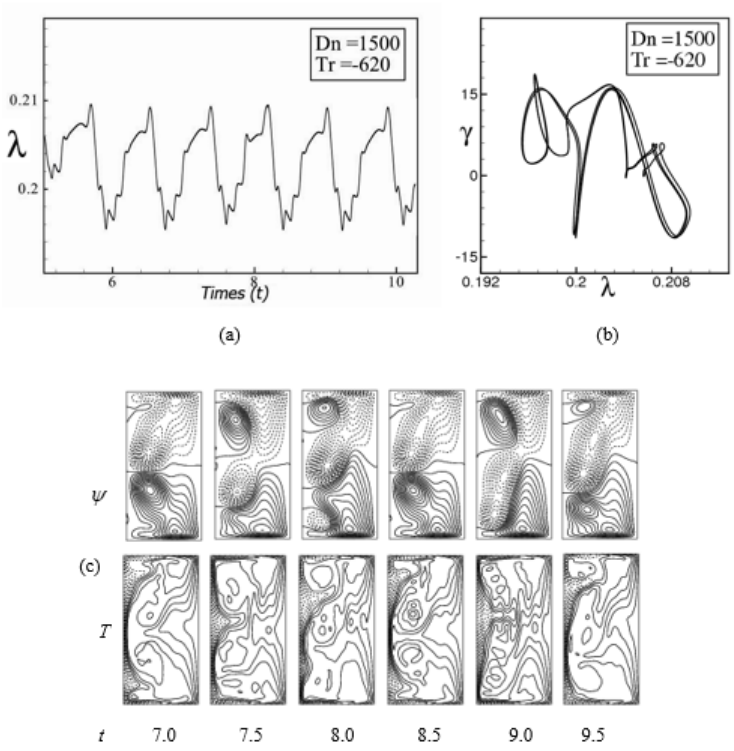


**Fig. 6.** Time-progress, phase-space and streamlines for Tr = -620 and $\delta = 0.5$. (a) Time advancement of $\lambda$, (b) Phase-portrait, (c) Contour plots of secondary flow (top), energy distribution (bottom) for $7.0 \leq t \leq 9.5$.

## Role of secondary vortices on convective heat transfer (CHT)

The influence of secondary vortices on the flow characteristics is presented in this section. In order to see the effects of secondary vortices on CHT, secondary flow pattern and temperature distributions are investigated at some monitoring points of Tr with respect to the steady-state, periodic/multi-periodic and chaotic solutions as presented in Fig. 10. Figures 10(a), 10(b) and 10(c) represent secondary flow pattern and isotherms (temperature profile) for the chaotic solutions at Tr = -50, -100, -300, -500, -600 and -620, periodic or multi-periodic solutions at Tr = -620, -670 and -680 and steady-state solution at Tr = -700 respectively, where it is clearly observed from Figure10 that maximum vortices (four- to six-vortex) exist in the chaotic solution i.e. the number of secondary vortices is strongly dependent on the flow state which is chaotic and recognized that chaotic flows enhance HT more effectively than the other flow transition behaviors. When the Dean vortices that get generated near the outer wall of the duct and the secondary flow becomes stronger and then heat transfer occurs at a great deal than usual (Chandratilleke and Nursubyakto [8]). In this regard, it is worth mentioning that irregular oscillation of the isothermal flows through a CRD has been observed experimentally by Ligrani and Niver [34] for the large aspect ratio.

## 5. Validation test

To be sure the accuracy of the present numerical results are validaited with the experimental studies performed by some authors from one aspects,namely, the streamlines of secondary flow. The streamlines of secondary flow of the present study has been compared with experimental data obtained by Yamamoto et al. [19] using visualization method for rotating curved square duct of curvature $\delta = 0.03$ for the negative rotation at Tr = -150 (Fig. 11(a)). In this study, however, we perform flow characteristics for the same configaration (not the three walls only), and compare our results with the existing results of Yamamoto et al. [7]. On the other hand, the experimental secondary flow patterns of the fluid had been explored by Chandratilleke [35] as presented in Fig. 11(b) for the flow through a stationary curved rectangular duct of aspect ratio 2. It is demonstrated that the streamlines of secondary flow which is found by adjusting the parameter with the experiments are identical. Therefore, our numerical results have a good matching with the experimental investigations. Unfortunately, no data exactly describing the full experimental data seems available for the rotating curved rectangular configuration.

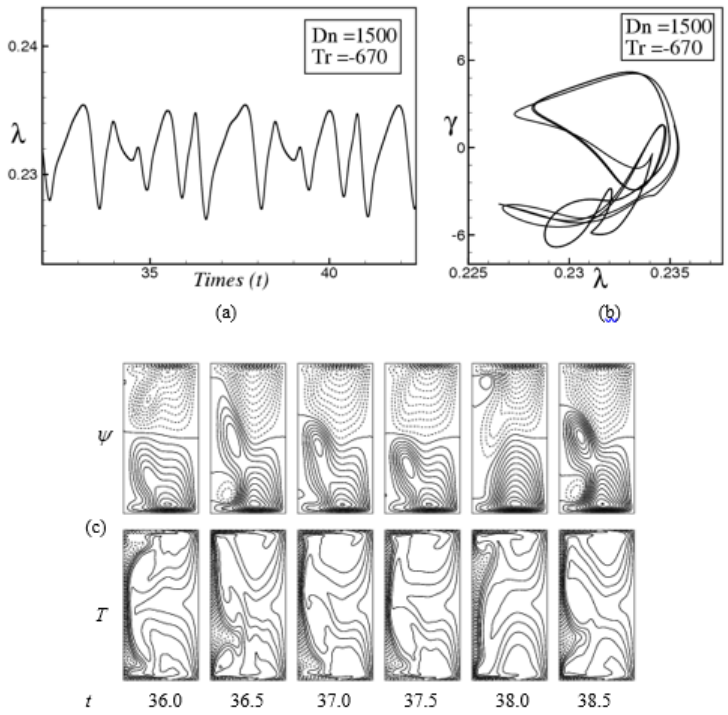


**Fig. 7.** Time-progress, phase-space and streamlines for Tr = -670 and $\delta = 0.5$. (a) Time advancement of $\lambda$, (b) Phase-portrait, (c) Contour plots of secondary flow (top), energy distribution (bottom) for $36.0 \leq t \leq 38.5$.

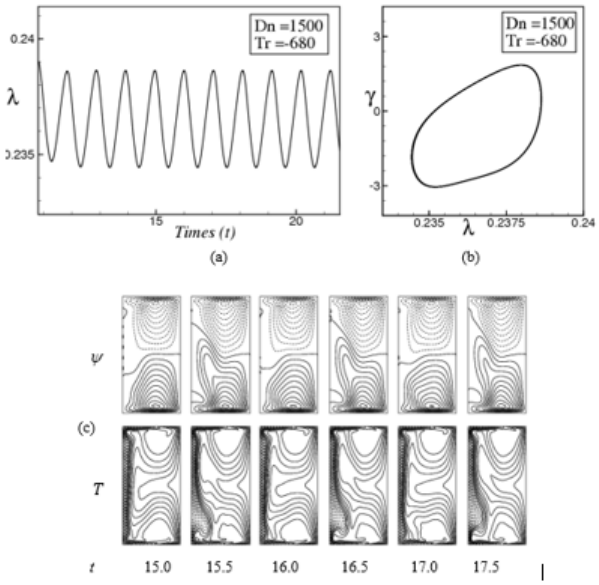


**Fig. 8.** Time-progress, phase-space and streamlines for Tr = -680 and $\delta = 0.5$. (a) Time advancement of $\lambda$, (b) Phase-portrait, (c) Contour plots of secondary flow (top), energy distribution (bottom) for $15.0 \leq t \leq 17.5$.

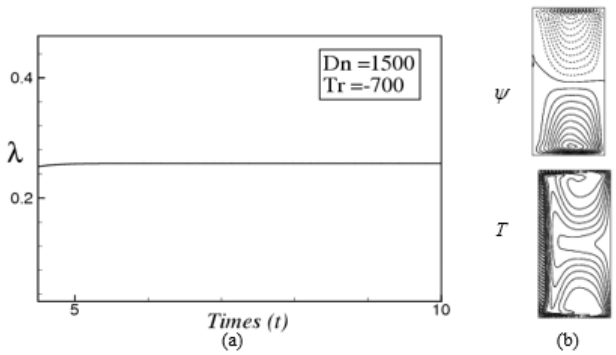


**Fig. 9.** Time-progress and streamlines for Tr = -700 and $\delta$ = 0.5. (a) Time advancement of $\lambda$, (b) Contour plots of secondary flow (top), energy distribution (bottom) at t = 10.

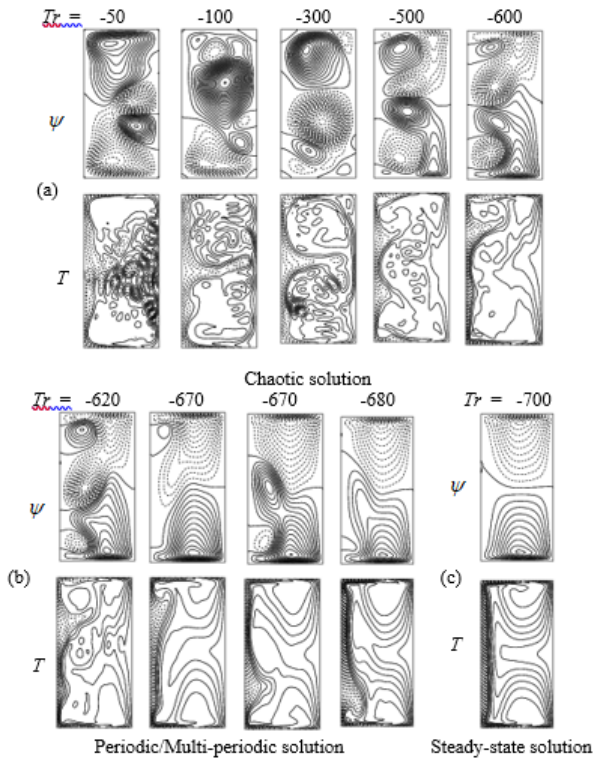


**Fig. 10.** Streamlines (top) and isotherm (bottom) for the steady-state, periodic/multi-periodic and chaotic solution for various negative vales of Tr at Dn = 1500 and curvature 0.5

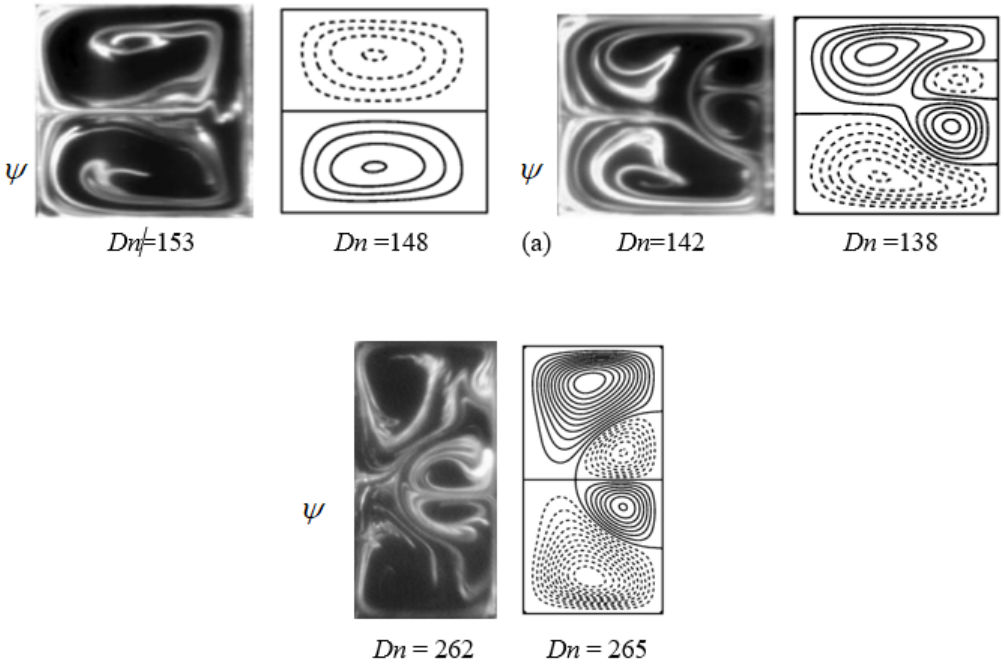


**Fig. 11.** Experimental vs. numerical results. (a) Streamlines of secondary flow at Tr = -150. Experimental result by Yamamoto et al. [7] (left) and numerical result by the authors (right), (b) Experimental result by Chandratilleke [35] (left) for curved rectangular duct flow of aspect ratio 2 and numerical result by the authors (right).

## 6. Conclusion

In this paper, a spectral-based numerical result of fully developed two-dimensional viscous incompressible fluid flow through a rotating curved rectangular duct has been conducted in the range of governing parameters as shown in Table 1. The entire process of origin, development and transition of flow motion has been described in detail. The characteristic flow phenomena such as counter-rotating vortices and transition regions have been presented covering a wide range of the Taylor number $-1000 \leq Tr < 0$ for negative rotation. Furthermore, a temperature difference is imposed across the vertical sidewalls for the Grashof number Gr = 100 where the outer-wall of the duct is heated while cooling from the inner wall, the other walls being thermally insulated to prevent heat loss. A detailed examination of flow transient behavior, time-advancement calculations are thoroughly performed and flow transition is precisely determined by obtaining phase space of the time-evolution results. It is observed that the chaotic, multi-periodic, periodic and steady-state flow regimes are observed for $-670 \leq Tr \leq -620$, and $-1000 \leq Tr \leq -700$ respectively. Therefore, the transition occurs from chaotic-state to multi-periodic oscillation between Tr = -600 and Tr = -620, multi-periodic to periodic between Tr = - 670 and Tr = -680 and periodic to steady-state between Tr = -680 and Tr = -700. It is found that maximum vortices (four- to six-vortex) exist in the chaotic region and recognized that chaotic flows enhance heat transfer more effectively than the other physically realizable solutions. This study also shows that there is a strong communication between the heating-induced buoyancy force and the centrifugal-Coriolis instability in the rotating curved passage that inspires fluid mixing and subsequently enhances heat transfer in the fluid. Finally, our numerical results are validated with experimental outcomes and it is found that there is a good agreement between the numerical and experimental investigations.

## References


[1] Dean W. R. (1927). Note on the motion of fluid in a curved pipe. Phil. Mag . 4(20), pp. 208-223.

[2] Humphrey J.A.C., Taylor A.M.K., Whitelaw J.H. (2006), Laminar flow in a square duct of strong curvature, J. Fluid Mech. 83(3), pp. 509–527.

[3] Ghia K.N., Sokhey J.S. (1977), Laminar incompressible viscous flow in curved ducts of rectangular cross-section, J. Fluids Eng. 99, pp. 640–648.

[4] Yanase S., Mondal R.N. and Kaga Y. (2005), Numerical Study of Non-Isothermal Flow with Convective Heat Transfer in a Curved Rectangular Duct, International Journal of Thermal Science, 44, pp. 1047-1060.

[5] Chandratilleke T.T, Nadim N. and Narayanaswamy R. (2013), Analysis of Secondary Flow Instability and Forced Convection in Fluid Flow Through Rectangular and Elliptical Curved Ducts, Heat Transfer Engineering, 34(14), pp. 1237-1248.

[6] Yanase S., Watanabe T. and Hyakutake T. (2008), Traveling-wave solutions of the flow in a curved-square duct, Physics of Fluids, 20, (124101).

[7] Yamamoto K, Wu. X, Hyakutake T. and Yanase S. (2004), Taylor–Dean flow through a curved duct of square cross section, Fluid Dynamics Research, 35, pp. 67–86.

[8] Chandratilleke T T. and Nursubyakto, (2003), Numerical prediction of secondary flow and convective heat transfer in externally heated curved rectangular ducts, International Journal of Thermal Sciences, 42, pp. 187–198.

[9] Mondal R.N., Watanabe T., Hossain M.A. and Yanase S. (2017), Vortex-Structure and Unsteady Solutions with Convective Heat Transfer Trough a Curved Duct, Journal of Thermophysics and Heat Transfer, 31(1), pp. 243-253.

[10] Chandratilleke T.T., Nadim N. and Narayanaswamy R. (2012), Vortex structure-based analysis of laminar flow behaviour and thermal characteristics in curved ducts, Int. J. Thermal Sciences, 59, pp. 75-86.

[11] Wang L. Q. (1997), Buoyancy-force-driven transitions in flow structures and their effects on heat transfer in a rotating curved channel, Int. J. Heat Mass Transfer, 40(2), pp. 223-235.

[12] Razavi S.E., Soltanipour H. and Choupani P. (2015), Second law analysis of Laminar Forced Convection in a rotating curved duct, Thermal Sciences, 19(1), pp. 95-107.

[13] Hasan M.S., Mondal R.N., Kouchi T. and Yanase S. (2019), Hydrodynamic instability with convective heat transfer through a curved channel with strong rotational speed, AIP Conference Proceedings 2121 (030006).

[14] Rivas G.A.R., Garcia E.C. and Assato M. (2014), Numerical Simulation of Turbulent Forced Convection Coupled to Heat Conduction in Square Ducts, Int. Review of Mechanical Engineering, 8(3). pp. 92-105.

[15] Norouzi M., Kayhani M.H., Nobari M.R.H. and Demneh M.K. (2009), Convective Heat Transfer of Viscoelastic Flow in a Curved Duct, World Academy of Science, Engineering and Technology, Int. J. Mechanical and Mechatronics Engineering, 3(8), pp. 921-927.

[16] Mondal R.N., Saha P.R, Poddar N.K. and Yanase S. (2015), Numerical prediction of Taylor-Dean flow through a rotating curved duct with constant curvature, Int. J. Adv. Appl. Math. and Mech. 3(1), pp. 10 – 23.

[17] Yanase S. and Nishiyama K., (1988). On the bifurcation of laminar flows through a curved rectangular tube, J. Phys. Soc. Japan, 57(11), pp. 3790-3795.

[18] Nazeer G., Islam S., Shigri S.H., Saeed S., (2019), Numerical investigation of different flow regimes for multiple staggered rows, AIP Advances, 9(3), 035247.
[19] Krishna C.V., Gundiah N., Arakeri J.H. (2017), Separations and secondary structures due to unsteady flow in a curved pipe, J. Fluid Mech. 815, pp. 26–59.
[20] Mondal R.N., Kaga Y., Hyakutake T. and Yanase S. (2006), Effects of curvature and convective heat transfer in curved square duct flows, Trans. ASME, Journal of Fluids Engineering, 128(9), pp. 1013-1022.
[21] Mondal R.N., Kaga Y., Hyakutake T. and Yanase S. (2007), Bifurcation diagram for two-dimensional steady flow and unsteady solutions in a curved square duct, Fluid Dynamics Research, 39, pp. 413–446.
[22] Mondal R.N., Islam M.S., Uddin K. and Hossain M.A. (2013), Effects of aspect ratio on unsteady solutions through curved duct flow, Applied Mathematics and Mechanics, 34(9), pp. 1107–1122.
[23] Islam M.Z., Mondal R.N., Rashidi M.M. (2017), Dean-Taylor flow with convective heat transfer through a coiled duct, Computers and Fluids, 149, pp. 41-55.
[24] Iva L.M, Hasan M.S., Paul S.K., Mondal R.N. (2018), MHD free convection heat and mass transfer flow over a vertical porous plate in a rotating system with hall current, heat source and suction, Int. J. Adv. Appl. Math. and Mech. 5(4), pp. 49 – 64
[25] Chandratilleke T.T., Nadim N., Narayanaswamy R. (2012), Vortex structure-based analysis of laminar flow behavior and thermal characteristics in curved ducts, Int. J. Therm. Sci. 59, pp. 75–86.
[26] Niemann M., Navarro R. A. B.,Saini V., Fröhlich J. (2018), Buoyancy impact on secondary flow and heat transfer in a turbulent liquid metal flow through a vertical square duct. Int. J. Heat and Mass transfer, 125, pp. 722-748.
[27] Sekimoto A., Kawahara G., Sekiyama K., Uhlmann M., Pinelli A. (2011), Turbulence and buoyancy-driven secondary flow in a horizontal square duct heated from below, Physics of Fluids, 23, pp. 1-19.
[28] Hasan M.S., Mondal R.N. and Lorenzini G. (2019), Numerical Prediction of Non-isothermal Flow with Convective Heat Transfer through a Rotating Curved Square Channel with Bottom Wall Heating and Cooling from the Ceiling, Int. J. Heat and Technology, 37(3), pp. 710-720.
[29] [Hasan M.S., Mondal R.N. and Lorenzini G. (2019), Centrifugal Instability with Convective Heat Transfer through a Tightly Coiled Square Duct, Mathematical Modelling of Engineering Problems, 6(3), pp. 397-408.
[30] Roy S.C., Hasan M.S. and Mondal R.N. (2020), On the Onset of Hydrodynamic Instability with Convective Heat Transfer through a Rotating Curved Rectangular Duct, Mathematical Modelling of Engineering Problems, 7(1), pp.31-44.
[31] Gottlieb D. and Orazag S.A. (1977), Numerical Analysis of Spectral Methods, Society for Industrial and Applied Mathematics, Philadelphia.
[32] Lorenz E.N. (1963), Deterministic non-periodic flow. J. Atmos. Sci, 20, 130-141.
[33] Ruelle D. and Takens F. (1971), On the nature of turbulence, Commun. Math. Phys., 20, pp. 167–192.
[34] Ligrani P.M. and Niver R.D. (1988), Flow visualization of Dean vortices in a curved channel with 40 to 1 aspect ratio, Phys. Fluids, 31, pp. 3605.
[35] Chandratilleke T.T. (2001), Secondary flow characteristics and convective heat transfer in a curved rectangular duct with external heating. 5th World Conference on Experimental Heat Transfer, Fluid Mechanics and Thermodynamics [ExHFT-5], Thessaloniki, Greece.